ENVIRONMENTAL RESEARCH
LETTERS

PURPOSE-LED PUBLISHING™

LETTER • OPEN ACCESS

A local meteoric water line for interior Alaska constrains paleoclimate from 40 000 year old relict permafrost

To cite this article: Thomas A Douglas *et al* 2025 *Environ. Res. Lett.* **20** 024029

IOP Publishing Environ. Res. Lett. 20 (2025) 024029 https://doi.org/10.1088/1748-9326/ada16b

ENVIRONMENTAL RESEARCH
LETTERS

OPEN ACCESS

RECEIVED
2 August 2024

REVISED
30 October 2024

ACCEPTED FOR PUBLICATION
19 December 2024

PUBLISHED
21 January 2025

LETTER

A local meteoric water line for interior Alaska constrains paleoclimate from 40 000 year old relict permafrost

Thomas A Douglas[1,*], **Amanda J Barker**[1], **Alistair J Monteath**[2] **and Duane G Froese**[3]

[1] US Army Cold Regions Research and Engineering Laboratory, 9th Avenue, Building 4070, Fort Wainwright, AK, 99709, United States of America
[2] British Antarctic Survey, Natural Environment Research Council, Cambridge, United Kingdom
[3] Department of Earth and Atmospheric Sciences, University of Alberta, Edmonton, AB, Canada
[*] Author to whom any correspondence should be addressed.

E-mail: Thomas.A.Douglas@usace.army.mil

Keywords: permafrost, paleoclimate, stable isotopes, ice wedge

Supplementary material for this article is available online

Abstract

Anthropogenic climate warming is degrading permafrost across interior Alaska. Information from past warming events provides long-term perspectives for future trajectories; however, late Quaternary seasonal temperatures are poorly constrained. We have established a stable water isotope meteoric water line for interior Alaska and measured stable water isotope values from 126 permafrost cores representing different ice types deposited over the past ∼40 ka (thousand years before 1950 CE). Samples represent two late Quaternary warm periods: marine isotope stage three (MIS3; 57–29 ka) and the Holocene (11.7 ka-present). Older samples provide insight into local climatic conditions slightly before the first archeological evidence for Paleolithic hunter-gatherers in the region. From permafrost ice we calculate that summer temperatures warmed by ∼10 °C between late MIS3 and today, with six degrees of warming between 40–30 ka and 3 ka and an additional 4 °C of warming since 3 ka. Half this recent 4 °C warming has occurred over the past 70 years.

1. Introduction

Interior Alaska (figure 1) is underlain by discontinuous permafrost ranging in thickness from a few meters to 50 m (Jorgenson *et al* 2001, Douglas *et al* 2021). Roughly half of this permafrost represents late Pleistocene ice and organic carbon-rich 'yedoma' formed through ice cementation of windblown loess (Strauss *et al* 2017). Pore ice cementing this loess comprises soil pore water, predominantly summer rain, that drained through the seasonally thawed 'active layer' and was subsequently frozen (Throckmorton *et al* 2016, Porter and Opel 2020, Kanevskiy *et al* 2022). This permafrost also contains ice wedges formed over hundreds to thousands of years as water from spring snowmelt filled cracks and froze (Lachenbruch 1962). In some places, permafrost has been replaced with younger deposits of soil and water. This material, likely mobilized by surface water during summer erosion events, subsequently froze to create 'thermokarst cave ice' (Douglas *et al* 2011, Kanevskiy *et al* 2017). It represents paleoprecipitation (summer meteoric water) from when the permafrost was eroded and replaced with surface water.

Stable water isotopes of hydrogen (δ^2H) and oxygen (δ^{18}O) in permafrost ice have been used to infer paleoclimatic conditions when rain or snow melt water was frozen and incorporated into the permafrost record (Mackay and Dallimore 1992, Vasil'Chuk and Vasil'Chuk 1997, Porter *et al* 2016, Opel *et al* 2018, Porter and Opel 2020, Vasil'chuk and Budantseva 2021, Wetterich *et al* 2021, Monteath *et al* 2023). A first step is to measure the stable water isotope composition of modern snow and rain to calculate a local meteoric water line (LMWL; Putman *et al* 2019). Once the LMWL has been established, inferences about paleoclimatic conditions can be made from permafrost ice types representing meteoric water from different seasons or time periods (Porter *et al* 2016).

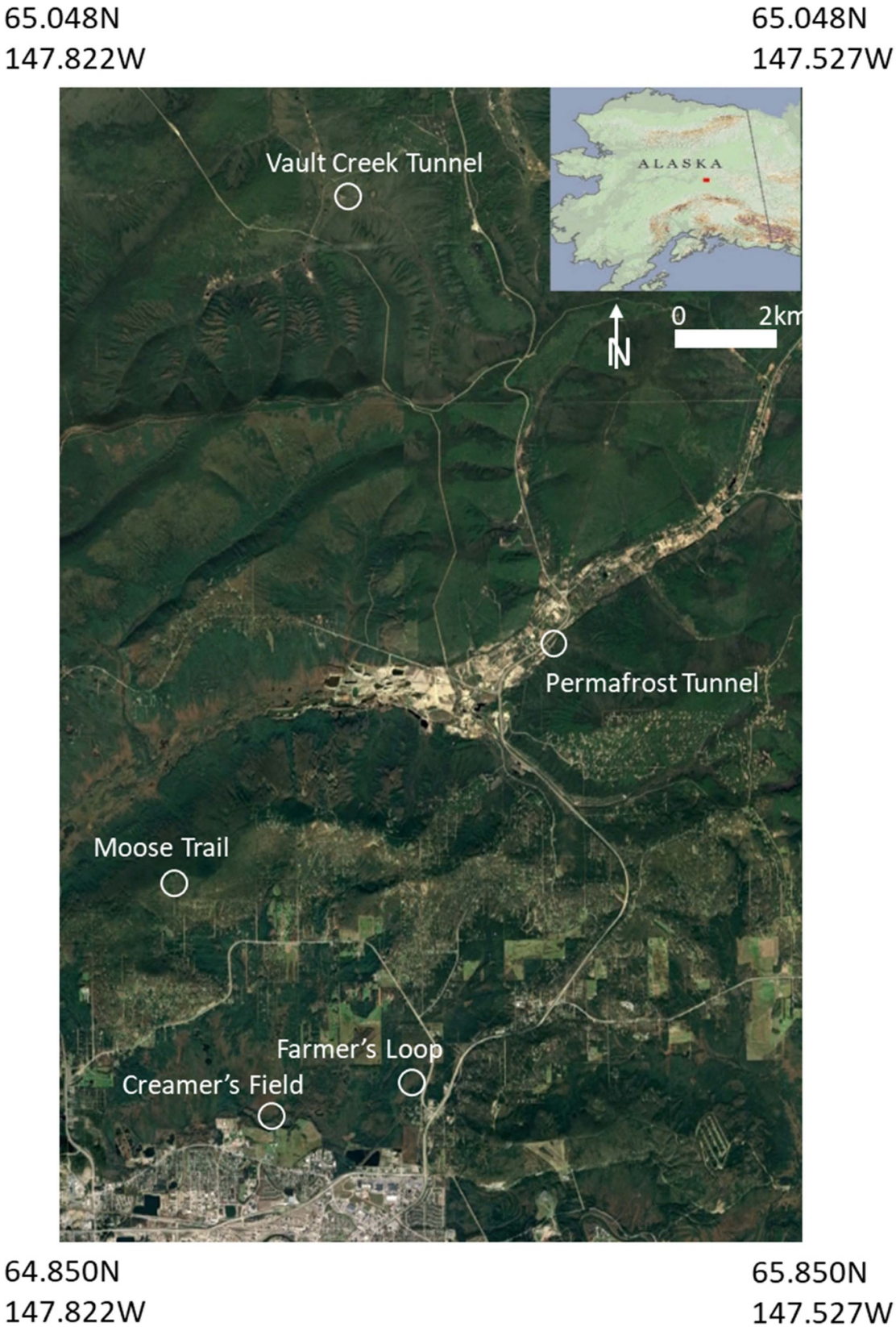

Figure 1. An image of the Fairbanks area identifying the locations of field sites in this study. Map data © 2020 Google.

In this study, we establish the first stable water isotope MWL for interior Alaska from 238 snow and rain samples. We also use stable water isotope values from 126 permafrost cores representing varied permafrost ice deposited over the past ~40 ka (thousand years before 1950 CE) to estimate seasonal paleotemperatures at multiple time periods. Our principal study site, the U. S. Army Cold Regions Research and Engineering Laboratory (CRREL) permafrost tunnel, includes deposits from two late Quaternary warm

periods: marine isotope stage three (MIS3) (∼57–29 ka; Lisiecki and Raymo 2005) and latest Pleistocene warming (∼15–11.7 ka), which coincided with the collapse of the Laurentide–Cordilleran ice complex and the first archeological evidence for Paleolithic hunter-gatherers in interior Alaska (Potter *et al* 2017). Using relationships between unique permafrost ice types representing snow melt and summer precipitation and their stable water isotope values, we calculate mean summer and winter temperatures at time periods between ∼40 ka and the present and place these into the context of recent and projected future climate warming in the area.

2. Field sites and methods

2.1. Snow and rain sample collection

Snow samples were collected from the surface of a 1.5 m high table at the Moose Trail site (64.905° N, 147.799° W; 313 m elevation) 8 km northwest of Fairbanks, Alaska (figure 1, supplemental table 1). The table provided low thermal gradient conditions and prevented redistribution of water vapor (Taillandier *et al* 2007). Samples were collected during events or within no more than 6 h following cessation of snowfall. The table was cleared following each sampling event. A total of 203 fresh snowfall samples were collected between fall 2003 and spring 2013. Some samples represent different periods during the same multi-day storm, while others represent an entire snowfall event. Not every event was collected during the decade of sampling. Between spring 2010 and fall 2013, 35 wet precipitation samples were collected from a 1 L narrow-mouth high-density polyethylene bottle with a 20 cm diameter funnel cap attached to the top of a 2 m pole. The bottle was housed inside a wooden box so only the top of the funnel was exposed. Water was collected within at most 12 h of cessation of any precipitation event. The bottle was emptied after each sample collection and each sample represents no more than 24 h of wet precipitation. Repeat analysis of rainwater from a sample bottle exposed over 2 weeks yielded stable water isotope values that did not change more than the values for analytical precision. As with snow samples, some rain was collected multiple times during an event while other samples represent an entire event. Not every wet precipitation event was collected during the 3-year sampling period.

2.2. Permafrost sample collection

Pore ice in silt, massive ice wedges and thermokarst cave ice were collected from two subsurface tunnels north of Fairbanks (figure 1). The CRREL permafrost tunnel (64.951° N, 147.621° W, 263 m elevation) provides access to permafrost from periods between ∼45–30 ka and ∼14 ka (Hamilton *et al* 1988, Mackelprang *et al* 2017, Kanevskiy *et al* 2022) to the modern age above the CRREL permafrost tunnel (Douglas *et al* 2021). The nearby Vault Creek tunnel (65.032° N, 147.706° W, 232 m elevation) provides access to ice wedges estimated to have formed between 50 and 25 ka (Meyer *et al* 2008, Schirrmeister *et al* 2016). A 10 cm diameter, 40 cm long carbide-tipped corer was used to collect cores from the two tunnels in 2016. Surface samples were collected with an 8 cm diameter, 1.2 m SIPRE corer in late winter and spring 2018 from above the CRREL permafrost tunnel and nearby Farmer's Loop Permafrost Experiment Station (64.877° N, 147.674° W, 135 m elevation) and Creamer's Field Migratory Waterfowl Refuge (64.868° N, 147.738° W, 135 m elevation).

2.3. Stable isotope analyses of precipitation and permafrost ice

Stable isotopes of hydrogen and oxygen were measured from precipitation collected between 2003 and 2011 using a Thermo Delta V mass spectrometer with a high-temperature conversion elemental analyzer pyrolysis oven (Thermo Scientific Waltham, Massachusetts) at the University of Alaska Fairbanks Stable Isotope Facility. We report mean values of triplicate analyses. Multiple analyses of standards and replicate analyses of samples yielded a precision of ±0.4‰ for oxygen (δ^{18}O) and ±2.0‰ for hydrogen isotopes (δD). Data are reported in per mil (‰) referenced to Vienna Standard Mean Ocean Water.

Stable isotopes of hydrogen and oxygen in precipitation samples collected from 2012 onward and all permafrost samples were measured by wavelength-scanned cavity ringdown spectroscopy on a Picarro L2120i (Sunnyvale, California) at the CRREL Geochemistry Laboratory at Fort Wainwright, Alaska. Standards and samples were injected into the analyzer for seven separate analyses. Measurements from the final three sample injections were used to calculate the mean and standard deviation for each sample. Stable isotope values are reported in standard per mil notation. Repeat analyses of standards representing a range of values spanning the samples were used to calibrate analytical results with an estimated precision of ±0.2‰ for δ^{18}O and ±0.5‰ for δD.

2.4. The present climate of interior Alaska

Fairbanks currently has a mean annual air temperature of −2 °C (Jorgenson *et al* 2020) with mean monthly temperatures ranging from 20 °C in summer to −20 °C in winter (Alaska Climate Research Center 2022). Typical annual precipitation is 28 cm water equivalent with ∼45% as snow (Liston and Hiemstra 2011). Based on decadal mean annual temperatures, the area warmed by 2.2–2.4 °C between the 1930s–1940s and 2010–2019 (NOAA

National Centers for Environmental Information 2022). Mean summer temperatures (1 May to 10 October) warmed ~1.7 °C and mean winter temperatures (11 October to 30 April) warmed 2–4 °C over this timeframe (National Oceanographic and Atmospheric Administration 2022).

3. Results and discussion

3.1. Stable water isotope composition of modern precipitation

Stable water isotope values for snow and rain collected near Fairbanks, Alaska, are summarized in figure 2. Summer precipitation has more enriched $\delta^{18}O$ values (mean −17.3‰, standard deviation 2.0‰) than winter precipitation (mean −26.7‰, standard deviation 5.2‰). The dataset establishes a LMWL (using mean monthly averages) with the equation $\delta^2H = 7.6\delta^{18}O - 16.5‰$ ($r^2 = 0.99$). The slope is close to the global meteoric water line (GMWL) of $\delta^2H = 8.17\delta^{18}O + 10.35‰$ (Rozanski *et al* 1993). Stable hydrogen and oxygen isotopes are strongly correlated for summer (wet precipitation best fit; $N = 31$; $\delta^2H = 6.5\delta^{18}O - 23.7‰$; $r^2 = 0.88$) and winter (snow best fit; $N = 207$; $\delta^2H = 8.0\delta^{18}O + 12.9‰$; $r^2 = 0.98$). We calculated a summer (rain) MWL from rain samples and a winter (snow) MWL from snow samples to highlight the seasonal character of the stable water isotope relationships in snow versus rain (Paulsson and Widerlund 2020). The summer best-fit line exhibits a depletion in heavy isotopes (^{18}O, D) compared with winter and the GMWL.

Figure 3 and supplemental tables 1 and 2 highlight relationships between stable oxygen isotope values of different types of precipitation and the air temperature when samples were collected. Winter air temperatures span more than twice the range of summer temperatures, and snow $\delta^{18}O$ values cover a far wider range (23.7‰) than those for rain (7.3‰). This wider range may be explained by the larger population of winter samples compared with summer. Coefficient of determination values between air temperature at sample collection and the $\delta^{18}O$ value of rain ($r^2 = 0.04$) and snow ($r^2 = 0.22$) do not indicate strong statistical significance. Due to the lack of a strong correlation between $\delta^{18}O$ and air temperature in our winter and summer samples and the absence of any nearby long-term record of stable isotopes in precipitation with which to compare them (e.g. Porter *et al* 2019), we use relationships between $\delta^{18}O$ and air temperature across a broader region of Alaska calculated by Lachniet *et al* (2016) for the mean temperature of the coldest quarter. They report linear correlations between $\delta^{18}O$ and winter season temperature ($r = 0.73$; 0.31‰ °C^{-1}) and mean annual temperature ($r = 0.71$; 0.60‰ °C^{-1}).

Relationships between δD and $\delta^{18}O$ in each sample can be explored further by calculating deuterium excess ($d = \delta^2H - 8\delta^{18}O$; Dansgaard 1964). The GMWL has a d-excess of 10% and departures identify non-equilibrium fractionation of ^{18}O and ^{16}O (Craig 1961). Deuterium excess values for snow and rain (supplemental figure 1, following Fritz *et al* 2022) do not show strong relationships with δD. However, the variability of rain deuterium excess values is significantly lower than those for snow [analysis of means with significance level (α) of 0.05]. Deuterium excess calculated from summer precipitation and about half the winter precipitation samples fall below 10‰, suggesting that evaporative processes occurred in winter precipitation air masses because the lighter $^1H^2H^{16}O$ molecule is preferentially evaporated into the vapor phase while the heavier $^1H^1H^{18}O$ molecule is retained in the liquid phase (Pfahl and Sodemann 2014). A lower d-excess in summer rain compared with winter snow suggests post-precipitation evaporative processes.

3.2. Paleoclimate conditions calculated from interior Alaska permafrost

Relationships between $\delta^{18}O$ of modern precipitation and paleoprecipitation can be used to calculate seasonal temperature differences between the time when a permafrost ice type was deposited and modern precipitation. We note that over long timescales stable water isotope values of precipitation can be affected by the changing isotopic composition of marine waters providing the precipitation (Porter *et al* 2019) and changes in climate, moisture sources and storm trajectories (Akers *et al* 2017). For example, opening of the Bering Strait ~12 ka changed climate and moisture sources during the Younger Dryas period in northern Alaska (Meyer *et al* 2010). Closure of the Bering Strait ~35 ka may have altered precipitation sources for interior Alaska (Farmer *et al* 2023).

The isotopic composition of seawater varies over time (Porter and Opel 2020). During MIS4 and MIS3/2, when ice sheets stored far more water than they do today, the glacial ocean was enriched in heavy isotopologues (Porter *et al* 2016). The majority of our samples represent MIS3. As such, our samples are corrected for an offset of +0.6‰ relative to today for $\delta^{18}O$ and +5‰ for δD (Rohling *et al* 2014, Porter *et al* 2016). This seawater correction makes our estimates of paleotemperatures slightly colder and modern temperatures relatively warmer than what would be calculated without the correction. Where we provide stable water isotope values for MIS3 age samples we provide both the raw and corrected values. It is possible that pore ice includes some cold season meteoric water that migrated downward through micro-cracks (Mackay 1983) and thus could represent annual precipitation (Porter and Opel 2020). This would bias

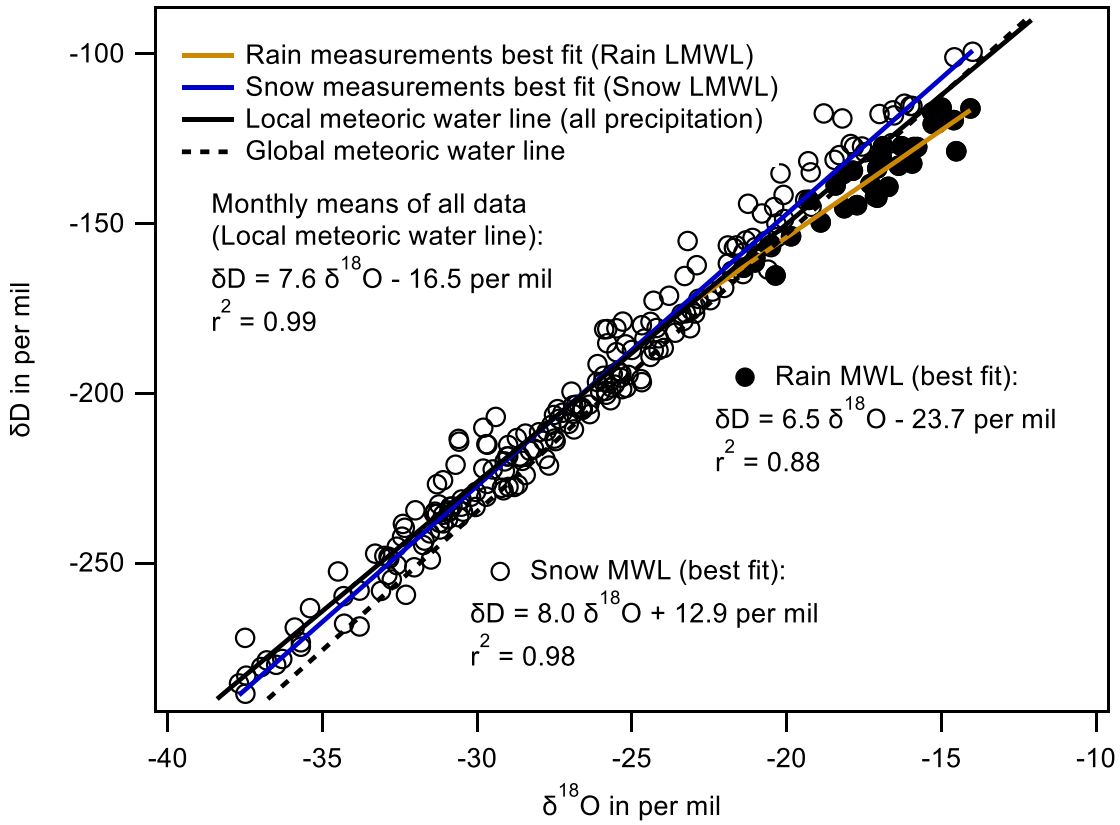

Figure 2. Stable water isotope values for 207 snow samples collected from 2004–2013 and 31 rain samples collected from 2010–2013. Mean monthly values were used to calculate the local meteoric water line (LMWL) with the linear fit equation and coefficient of determination for the two populations. The local, rain and snow meteoric water lines (MWLs) and their equations are shown along with the global meteoric water line (Rozanski *et al* 1993).

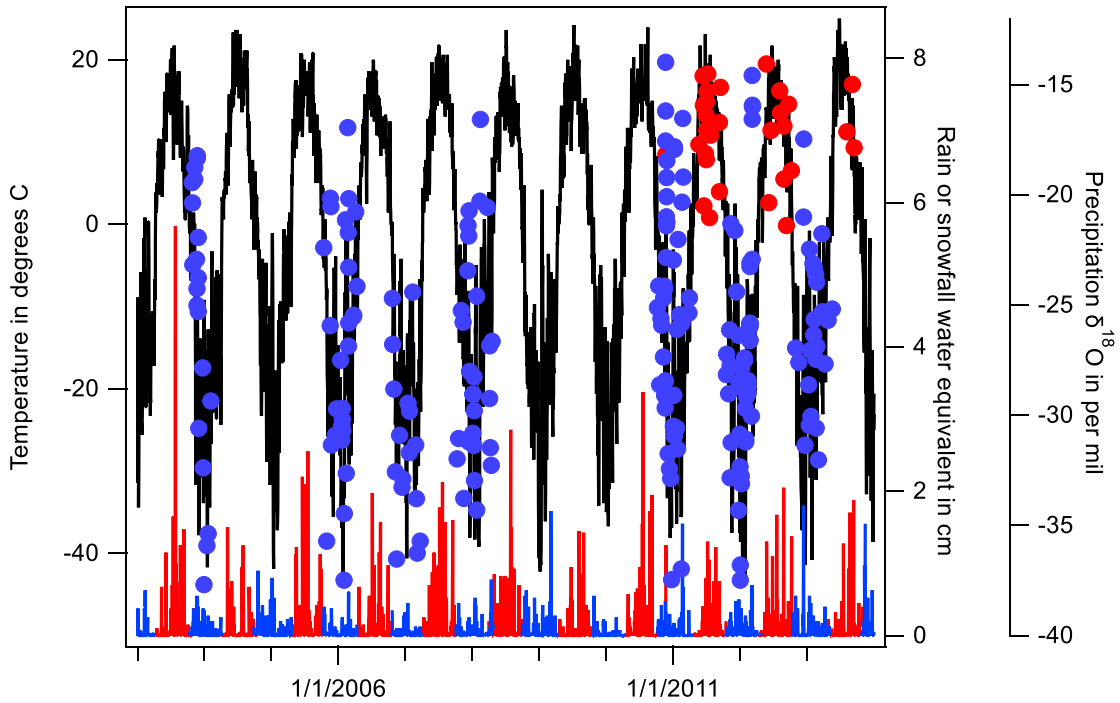

Figure 3. Mean daily air temperatures and rain or snow water equivalent from Fairbanks airport (shown as a black line) with precipitation $\delta^{18}O$ values during the sampling period of this study (snow samples shown in blue, rain samples shown in red). The mean air temperature from 1903–2020 was −2.8 °C. The mean annual air temperature from 2003 to 2014 was −2.3 °C.

results towards more negative $\delta^{18}O$ values and anomalously colder apparent temperatures; however, there are no visible cryostructures in any samples to suggest that downward migration through the pore ice was widespread at our sampling locations.

3.3. Stable water isotope composition of permafrost and active layer soils

Stable water isotope values for 126 permafrost and active layer samples from four sites around Fairbanks are plotted with rain and snow MWLs in figure 4. Ice wedges from both tunnels yield stable water isotope values representative of winter precipitation, while thermokarst cave ice represents predominantly summer precipitation. Pore ice aligns with either summer precipitation (above the CRREL permafrost tunnel and the Creamer's Field and Farmer's Loop sites) or a mix of summer and winter precipitation. For example, CRREL permafrost tunnel pore ice plots between winter and summer MWLs, but since it was deposited 40–30 ka (Kanevskiy *et al* 2022) during a colder climate it is likely that summer precipitation had lower δD and $\delta^{18}O$ values than today. Samples included 82 cores from the CRREL permafrost tunnel (supplemental figure 2) representing ice wedges, thermokarst cave ice and pore ice cemented silt. Supplemental figure 3 provides a cross section of the CRREL permafrost tunnel that summarizes ages and oxygen stable isotope values of different permafrost and soil samples. Additional data summaries are provided in supplemental tables 3 and 4. We also sampled three ice wedges from the Vault Creek tunnel that are similar to the CRREL permafrost tunnel. Supplemental table 5 synthesizes all CRREL permafrost tunnel published ages.

Since ice wedges form over hundreds to thousands of years and individual foliations are typically only a few millimeters wide, our 8 cm diameter cores represent multiple years of ice wedge growth (Lachniet *et al* 2012). None of our ice wedge samples exhibited any signs of post-formation melting (Douglas *et al* 2011) and we avoided sampling boundaries with pore-ice cemented silt or thermokarst cave ice. Ice wedge $\delta^{18}O$ values from 46 CRREL permafrost tunnel samples (−29.0‰ to −23.4‰, mean of −26.2 ± 1.3‰, corrected mean value of −26.8‰) and three samples from the Vault Creek tunnel (−28.3‰ to −24.4‰, mean of −26.4 ± 2.0‰, corrected mean value of −27‰) are statistically significantly similar to one another (analysis of means with $\alpha = 0.05$). These are similar to previously reported measurements from the CRREL permafrost tunnel (Douglas *et al* 2011, Lachniet *et al* 2012, Kanevskiy *et al* 2022).

Ages of CRREL permafrost tunnel Pleistocene ice wedges are poorly constrained. Radiocarbon dating indicates that host sediments include a hiatus between ∼31 ka and ∼15 ka (Hamilton *et al* 1988, Kanevskiy *et al* 2022); however, epigenetic ice wedges may have formed during this depositional hiatus. A chronological investigation radiocarbon dated an ice wedge and overlying thermokarst cave ice (Lachniet *et al* 2012). Calibrated radiocarbon dates from particulate organic matter ($n = 10$) ranged between 35.2 ka and 32.5 ka, while calibrated radiocarbon dates from CO_2 ($n = 4$) and dissolved organic carbon ($n = 4$) ranged between 28.1 ka and 24.0 ka. Three calibrated radiocarbon dates from overlying thermokarst ice ranged between 31.1 ka and 21.5 ka. A more recent study (Kanevskiy *et al* 2022) radiocarbon dated 13 plant macrofossil remains trapped within thermokarst ice truncating ice wedges in the CRREL permafrost tunnel. These radiocarbon dates cluster tightly around 35 ka, suggesting that the majority of Pleistocene ice wedges formed during MIS3.

For winter precipitation, there is no significant difference between modern precipitation $\delta^{18}O$ (−26.7‰) and the ice wedges we sampled (−26.2 ± 1.3‰, corrected mean value of −26.8‰). The similarity between inferred ice wedge temperatures and modern temperatures strongly suggests that ice wedges in the CRREL permafrost tunnel are of MIS3 age as full glacial winter conditions are likely to have been substantially cooler than today (Porter *et al* 2016), or they contain some summer precipitation water (ice). If there was some rainwater mixed into these ice wedges during their formation the temperatures calculated from them would be higher than the true winter values.

For a more regional comparison, we note that our results differ from a study (Porter *et al* 2016) that used differences in modern $\delta^{18}O$ and $\delta^{18}O$ values from a ∼30 ka ice wedge in central Yukon to calculate that winter temperatures warmed by ∼13 °C. Calculations using pore ice samples at the same site showed that mean annual temperatures increased by ∼15 °C. The differences between our isotopic measurements and the Yukon ones may be caused by different ice wedge ages or different regional climate controls. If ice wedges in the CRREL permafrost tunnel are older than ∼35 ka, as suggested by overlying thermokarst cave ice, then they formed under a very different climate from the ice wedges analyzed in Yukon by Porter *et al* (2016) where glacial conditions were established by 30 ka (Zazula *et al* 2007). Alternatively, the Laurentide–Cordilleran ice sheet is likely to have had a strong local cooling effect on Yukon, although its exact extent at 30 ka is not well established (Kennedy *et al* 2010).

Since ice wedges are currently growing only in climates colder than modern Fairbanks (Kokelj *et al* 2011), temperatures were likely to be considerably colder during the formation of CRREL permafrost tunnel ice wedges. As was stated earlier, we do not have information on the isotopic composition of marine waters when the ice wedges formed so our

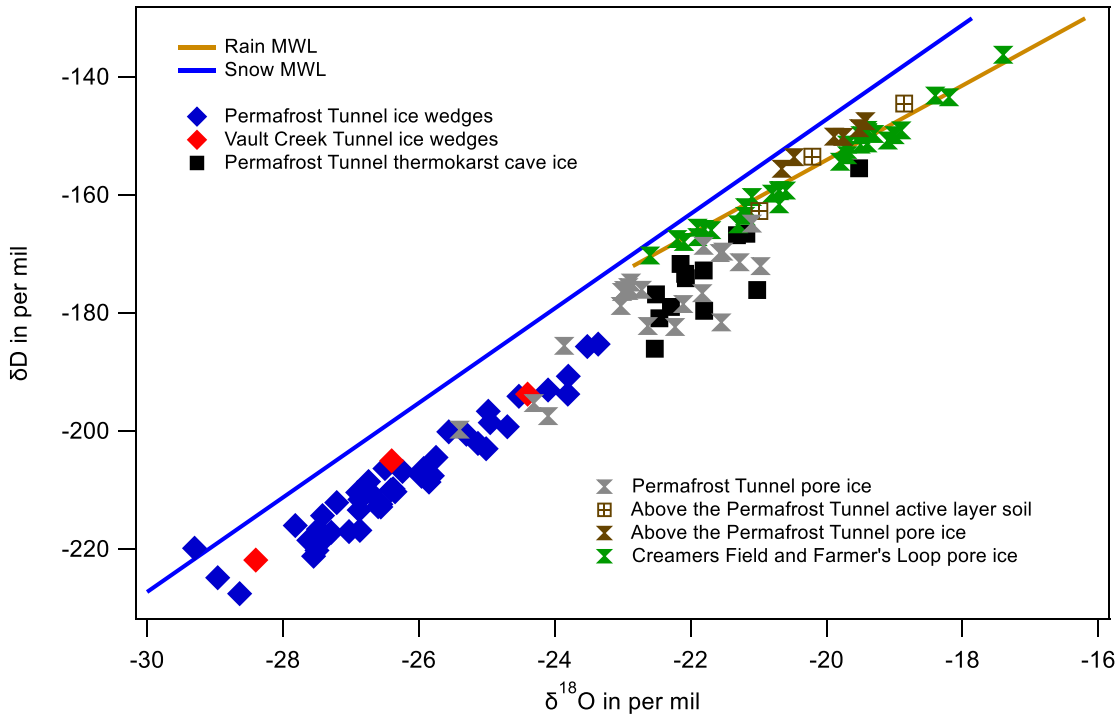

Figure 4. Stable water isotope values for all the permafrost samples collected at the field sites with the local meteoric water line (MWL) rain and snow local MWLs. Approximate ages of the different sample types: Permafrost Tunnel ice wedges (∼30–35 ka; Lachniet *et al* 2012, Kanevskiy *et al* 2022); Vault Creek Tunnel ice wedges (50–25 ka; Meyer *et al* 2008; Schirrmeister *et al* 2016); Permafrost Tunnel thermokarst cave ice (43–34 ka; Kanevskiy *et al* 2022); Permafrost Tunnel pore ice (40–30 ka; Barbato *et al* 2022, Kanevskiy *et al* 2022); above the Permafrost Tunnel active layer soil (modern; less than 500 years old); Above the Permafrost Tunnel pore ice and Creamer's Field and Farmer's Loop pore ice (these samples are from a maximum depth of 3 am and are thus ∼3 ka based on deposition rates of 1 mm year^{-1} ; Hamilton *et al* 1988, Douglas *et al* 2021).

temperature calculations provide minimum estimates and seawater correction would make estimates of paleotemperatures even colder.

Thermokarst cave ice from the CRREL permafrost tunnel represents predominantly summer season thermal and hydrological erosion and replacement of ice wedges and adjacent pore ice-cemented silt by surface water. This water froze over subsequent winters and has not melted since (Douglas *et al* 2011). Thirteen radiocarbon dates from wood in these thermokarst cave ice deposits yield ages from 43.5 ka to 34.1 ka, while the majority of ages (12 of the 13 dates) are ∼35 ka (Kanevskiy *et al* 2022). δ^{18}O measurements from thermokarst cave ice range from −27‰ to −19.5‰ with a mean of −22.5 ± 1.9‰ and corrected mean value of −23.1‰. A comparison can be made between the δ^{18}O value of these samples representing summer precipitation ∼35 ka (−22.5‰, corrected value of −23.1‰) and modern summer precipitation (−17.3‰) using the 0.60‰ °C^{-1} from Lachniet *et al* (2016). As stated earlier, there is a lack of a strong correlation between δ^{18}O and air temperature in our winter and summer samples and an absence of any nearby long-term record of stable isotopes in precipitation. As such, we use relationships between δ^{18}O and air temperature for a broader region of Alaska (Lachniet *et al* 2016). They report linear correlations between δ^{18}O and winter season temperature (r = 0.73; 0.31‰ °C^{-1}) and mean annual temperature (r = 0.71; 0.60‰ °C^{-1}). From this, we calculate a corrected summer season increase of 10 °C between ∼35 ka and the present.

Most pore ice inside the CRREL permafrost tunnel cements loessal soils from 40–30 ka (Kanevskiy *et al* 2022). The majority of this pore ice is structureless (i.e. no ice layers), which suggests minimal potential for cryostructural fractionation during freezing. Only a small section near the North Portal is known to be younger (Hamilton *et al* 1988, Kanevskiy *et al* 2022). Pore ice represents late summer precipitation when the active layer was at its maximum extent (Throckmorton *et al* 2016, Porter and Opel 2020). Their δ^{18}O values vary (−25.4‰ to −21.0‰, mean of −22.6 ± 1.1‰, corrected mean value of −23.2‰) suggesting variation in the summer precipitation stable isotopic composition during syngenetic permafrost aggradation. This may reflect MIS3 climate instability as seen in Greenland ice cores but which is poorly resolved in terrestrial sequences from Alaska/Yukon, and further study is needed to test this. A recent study of 37–31 ka pore ice collected throughout the CRREL permafrost tunnel reports the same

mean uncorrected δ^{18}O value of −22.6‰ (Kanevskiy *et al* 2022; corrected mean value of −23.2‰). All our pore ice samples are shifted to higher ^{18}O values compared with the summer MWL, consistent with ice wedge and thermokarst cave ice (figure 4). Using these samples, comparisons can be made between modern values and permafrost ice representing different time periods of paleoprecipitation and, likely, different moisture source regions and air mass trajectories (e.g. Meyer *et al* 2010, Lachniet *at el* 2016, Broadman *et al* 2020). Using our mean modern summer precipitation values (−17.3‰) and the relationship of 0.60‰ °C^{-1} (Lachniet *et al* 2016) we calculate that corrected mean summer temperatures increased by ∼10 °C from 40–30 ka to the present. This is the same value calculated for the summer temperature increase from thermokarst cave ice.

Quantitative summer temperature estimates for Alaska and Yukon during MIS3 are rare. The most common come from beetle assemblages with values derived using the mutual climatic range technique (e.g. Elias 2000, 2013). These quantitative estimates are limited by statistical biases (Bray *et al* 2006); however, dated MIS3 site summer temperatures were ∼4 °C colder than present. Chirinomid based summer temperature estimates provide a second data source. At Burial Lake, northwest Alaska, they suggest temperatures were ∼4 °C lower than modern values between 40 ka and 30 ka (Kurek *et al* 2009). Our summer temperature estimates are substantially cooler than these.

Relict pore ice from cores representing the upper 3 m of near-surface permafrost at the Creamer's Field and Farmer's Loop sites yields δ^{18}O values ranging from −22.5‰ to −17.5 ± 1.3‰ (mean −20.3‰) (supplemental tables 3 and 4 and supplemental figure 4). Based on loess deposition rates of ∼1 mm year^{-1} (Hamilton *et al* 1988, Douglas *et al* 2021) they represent frozen pore waters of ∼3 ka. Their δ^{18}O values are within the range of 58 surface water samples collected from the nearby Chena River (−23.3‰ to −19.4‰; Douglas *et al* 2013) and plot along the summer MWL. Deuterium excess in the surface active layer and pore ice (supplemental figure 5) confirms a modern summer meteoric water composition. However, far older CRREL permafrost tunnel pore ice (40–30 ka) has a significantly lower *d*-excess and δD values than these surface samples (analysis of means with $\alpha = 0.05$).

Using the δ^{18}O temperature relationship of 0.60‰ °C^{-1} (Lachniet *et al* 2016), the corrected ∼3.2‰ increase in summer precipitation δ^{18}O values between the 40 ka and 30 ka pore ice and the ∼3 ka to modern pore ice and pore waters equates to a 5 °C increase in summer temperatures over this time period. This is roughly half of the 10 °C warming between ∼40 ka and the present that we calculated from CRREL permafrost tunnel pore ice and thermokarst cave ice. The ∼2.5‰ increase in δ^{18}O values between young pore ice above the CRREL permafrost tunnel (3 ka; −20‰), young pore ice at Farmer's Loop and Creamer's Field (−20.3‰) and active layer samples above the CRREL permafrost tunnel (−20‰) compared with modern summer precipitation (−17.3‰) suggests a summer temperature increase of 4 °C between the last ∼1–3 ka and the present.

4. Conclusions

This study establishes the first LMWL for interior Alaska, providing a framework for comparing permafrost representing winter (ice wedges) and summer (thermokarst cave ice and pore ice) precipitation sources. Using the MWL and these changes in permafrost ice stable isotopes we established relationships between stable isotope values of precipitation and seasonal air temperatures over different time periods. Ice wedges represent winter precipitation during MIS3, thermokarst cave ice comprises summer precipitation ∼35 ka, older (40–30 ka) and younger (∼3 ka) pore ice represents summer precipitation and active layer soils contain modern precipitation. We find that during MIS3 winter temperatures were similar to today; however, summer temperatures were considerably cooler. Between 40–30 ka and the present both the thermokarst cave ice and pore ice suggest a warming of 10 °C. A comparison of 40–30 ka pore ice and ∼3 ka pore ice suggests that 5 °C of that warming occurred prior to 3 ka.

To place these paleotemperatures into context, almost half of the ∼5 °C of warming that occurred between ∼3 ka and the present can be accounted for by the ∼2 °C increase in mean annual temperature between the 1930s and 2020 (National Oceanographic and Atmospheric Administration 2022). However, it should be noted that more winter warming (4.3 °C) occurred since the 1930s compared with summer warming (1.4 °C; Alaska Climate Research Center 2022). Future climate scenarios project a 3–7 °C increase in mean annual air temperatures for the interior Alaska over the next 80 years (Walsh *et al* 2008). This means that the total climate warming projected to occur between the 1930s and 2100 of ∼9 °C is comparable to the total warming over the past 40 ka calculated in this study. Recent (last ∼20 years) warming in the area has led to widespread permafrost thaw (Douglas *et al* 2021, Farquharson *et al* 2022), and this is projected to continue into the future with near-surface permafrost likely to be absent in the study area by 2100 (Pastick *et al* 2015).

Data availability statement

Correspondence and requests for materials should be addressed to TAD. All data except stable water isotope

values of precipitation are provided in the supplemental information. All data provided in the supplemental information and stable water isotope values of precipitation are accessible at Zenodo using https://doi.org/10.5281/zenodo.10155689 ('Stable oxygen and hydrogen isotope values for permafrost ice, rain, and snow collected near Fairbanks, Alaska and a summary of all age dates from the CRREL Permafrost Tunnel').

Acknowledgments

This research was funded by the Strategic Environmental Research and Development Program (Projects RC-2110 and RC18-1170). We thank the numerous people who helped with soil and ice sample collection. Multiple reviewers provided comments on an earlier version of this manuscript but we specifically want to acknowledge Hanno Meyer and Sebastian Wetterich for their constructive comments and two anonymous reviewers. We acknowledge no real or perceived financial conflicts of interests for any author.

ORCID iDs

Thomas A Douglas https://orcid.org/0000-0003-1314-1905
Amanda J Barker https://orcid.org/0000-0003-0703-2702
Alistair J Monteath https://orcid.org/0009-0000-0199-9926
Duane G Froese https://orcid.org/0000-0003-1032-5944

References

Akers P D, Welker J M and Brook G A 2017 Reassessing the role of temperature in precipitation oxygen isotopes across the eastern and central United States through weekly precipitation-day data *Water Resour. Res.* **53** 7644–61

Alaska Climate Research Center 2022 Fairbanks International Airport (PAFA) historical data (available at: https://akclimate.org/data) (Accessed 15 January 2022)

Barbato R, Jones R, Douglas T, Doherty S, Messan K, Foley K, Perkins E, Thurston A and Garcia-Reyero N 2022 Not all permafrost microbiomes are created equal: Influence of permafrost thaw on the soil microbiome in a laboratory incubation study *Soil Biol. Biochem.* **167** 108605

Bray P J, Blockley S P, Coope G R, Dadswell L F, Elias S A, Lowe J J and Pollard A M 2006 Refining mutual climatic range (MCR) quantitative estimates of palaeotemperature using ubiquity analysis *Quat. Sci. Rev.* **25** 1865–76

Broadman E, Kaufman D S, Henderson A C, Malmierca-Vallet I, Leng M J and Lacey J H 2020 Coupled impacts of sea ice variability and North Pacific atmospheric circulation on Holocene hydroclimate in Arctic Alaska *Proc. Natl Acad. Sci. USA* **117** 33034–42

Craig H 1961 Isotopic variations in meteoric waters *Science* **133** 1702–3

Dansgaard W 1964 Stable isotopes in precipitation *Tellus* **16** 436–68

Douglas T A *et al* 2021 Recent degradation of interior Alaska permafrost mapped with ground surveys, geophysics, deep drilling, and repeat airborne LiDAR *Cryosphere Discuss.* **15** 1–39

Douglas T A, Blum J D, Guo L, Keller K and Gleason J D 2013 Hydrogeochemistry of seasonal flow regimes in the Chena River, a subarctic watershed draining discontinuous permafrost in interior Alaska (USA) *Chem. Geol.* **335** 48–62

Douglas T A, Fortier D, Shur Y I, Kanevskiy M Z, Guo L, Cai Y and Bray M 2011 Biogeochemical and geocryological characteristics of wedge and thermokarst-cave ice in the CRREL Permafrost Tunnel, Alaska *Permafr. periglacial Process.* **22** 120–8

Elias S A 2000 Late Pleistocene climates of Beringia, based on analysis of fossil beetles *Quat. Res.* **53** 229–35

Elias S A 2013 Beetle records/late Pleistocene of North America *Encyclopaedia of Quaternary Science* 2nd (Elsevier) pp 222–36

Farmer J R, Pico T, Underwood O M, Cleveland Stout R, Granger J, Cronin T M, Fripiat F, Martínez-García A, Haug G H and Sigman D M 2023 The Bering Strait was flooded 10,000 years before the Last Glacial Maximum *Proc. Natl Acad. Sci. USA* **120** e2206742119

Farquharson L M, Romanovsky V E, Kholodov A and Nicolsky D 2022 Sub-aerial talik formation observed across the discontinuous permafrost zone of Alaska *Nat. Geosci.* **15** 475–81

Fritz M, Wetterich S, McAlister J and Meyer H 2022 A new local meteoric water line for Inuvik (NT, Canada) *Earth Syst. Sci. Data Discuss.* **14** 57–63

Hamilton T D, Craig J L and Sellmann P V 1988 The Fox permafrost tunnel: a late Quaternary geologic record in central Alaska *Geol. Soc. Am. Bull.* **100** 948–69

Jorgenson M T, Douglas T A, Liljedahl A K, Roth J E, Cater T C, Davis W A, Frost G V, Miller P F and Racine C H 2020 The roles of climate extremes, ecological succession, and hydrology in repeated permafrost aggradation and degradation in fens on the Tanana Flats, Alaska *J. Geophys. Res.* **125** e2020JG005824

Jorgenson M T, Racine C H, Walters J C and Osterkamp T E 2001 Permafrost degradation and ecological changes associated with a warming climate in central Alaska *Clim. Change* **48** 551–79

Kanevskiy M, Shur Y, Bigelow N H, Bjella K, Douglas T A, Fortier D, Jones B M and Jorgenson M T 2022 Yedoma cryostratigraphy of recently excavated sections of the CRREL permafrost tunnel near Fairbanks, Alaska *Front. Earth Sci.* **9** 758800

Kanevskiy M, Shur Y, Jorgenson T, Brown D R, Moskalenko N, Brown J, Walker D A, Raynolds M K and Buchhorn M 2017 Degradation and stabilization of ice wedges: implications for assessing risk of thermokarst in northern Alaska *Geomorphology* **297** 20–42

Kennedy K E, Froese D G, Zazula G D and Lauriol B 2010 Last Glacial Maximum age for the northwest Laurentide maximum from the Eagle River spillway and delta complex, northern Yukon *Quat. Sci. Rev.* **29** 1288–300

Kokelj S V, Pisaric M F J and Burn C R 2011 Cessation of ice-wedge development during the 20th century in spruce forests of eastern Mackenzie Delta, Northwest Territories, Canada *Can. J. Earth Sci.* **44** 1503–15

Kurek J, Cwynar L C, Ager T A, Abbott M B and Edwards M E 2009 Late Quaternary paleoclimate of western Alaska inferred from fossil chironomids and its relation to vegetation histories *Quat. Sci. Rev.* **28** 799–811

Lachenbruch A H 1962 *Mechanics of Thermal Contraction Cracks and Ice-Wedge Polygons in Permafrost* (Geological Society of America) vol 70

Lachniet M S, Lawson D E and Sloat A R 2012 Revised ^{14}C dating of ice wedge growth in interior Alaska (USA) to MIS2 reveals cold paleoclimate and carbon recycling in ancient permafrost terrain *Quat. Res.* **78** 217–25

Lachniet M S, Lawson D E, Stephen H, Sloat A R and Patterson W P 2016 Isoscapes of δ^{18}O and δ^{2}H reveal

climatic forcings on Alaska and Yukon precipitation *Water Resour. Res.* **52** 6575–86
Lisiecki L E and Raymo M E 2005 A Pliocene-Pleistocene stack of 57 globally distributed benthic $\delta^{18}O$ records *Paleoceanography* **20** 17
Liston G E and Hiemstra C A 2011 The changing cryosphere: pan-Arctic snow trends (1979–2009) *J. Clim.* **24** 5691–712
Mackay J R 1983 Downward water movement into frozen ground, western Arctic coast *Can. J. Earth Sci.* **20** 120–34
Mackay J R and Dallimore S R 1992 Massive ice of the Tuktoyaktuk area, western Arctic coast, Canada *Can. J. Earth Sci.* **29** 1235–49
Mackelprang R, Burkert A, Haw M, Mahendrarajah T, Conaway C H, Douglas T A and Waldrop M P 2017 Microbial survival strategies in ancient permafrost: insights from metagenomics *ISME J.* **10** 2305–18
Meyer H, Schirrmeister L, Yoshikawa K, Opel T, Wetterich S, Hubberten H W and Brown J 2010 Permafrost evidence for severe winter cooling during the Younger Dryas in northern Alaska *Geophys. Res. Lett.* **37** L03501
Meyer H, Yoshikawa K, Schirrmeister L and Andreev A 2008 The Vault Creek Tunnel (Fairbanks region, Alaska)—a late Quaternary palaeoenvironmental permafrost record *Proc. Ninth Int. Conf. on Permafrost* pp 1191–6
Monteath A J *et al* 2023 Relict permafrost preserves megafauna, insects, pollen, soils and pore-ice isotopes of the mammoth steppe and its collapse in central Yukon *Quat. Sci. Rev.* **299** 107878
National Oceanographic and Atmospheric Administration 2022 National centers for environmental information station data for Fairbanks International Airport (available at: www.ncdc.noaa.gov/cdo-web)
Opel T, Meyer H, Wetterich S, Laepple T, Dereviagin A and Murton J 2018 Ice wedges as archives of winter paleoclimate: a review *Permafr. periglacial Process.* **29** 199–209
Pastick N J, Jorgenson M T, Wylie B K, Nield S J, Johnson K D and Finley A O 2015 Distribution of near-surface permafrost in Alaska: estimates of present and future conditions *Remote Sens. Environ.* **168** 301–15
Paulsson O and Widerlund A 2020 Pit lake oxygen and hydrogen isotopic composition in subarctic Sweden: a comparison to the local meteoric water line *Appl. Geochem.* **118** 104611
Pfahl S and Sodemann H 2014 What controls deuterium excess in global precipitation? *Clim. Past* **10** 771–81
Porter T J, Froese D G, Feakins S J, Bindeman I N, Mahony M E, Pautler B G, Reichart G J, Sanborn P T, Simpson M J and Weijers J W 2016 Multiple water isotope proxy reconstruction of extremely low last glacial temperatures in eastern Beringia (Western Arctic) *Quat. Sci. Rev.* **137** 113–25
Porter T J and Opel T 2020 Recent advances in paleoclimatological studies of Arctic wedge-and pore-ice stable-water isotope records *Permafr. periglacial Process.* **31** 429–41
Porter T J, Schoenemann S W, Davies L J, Steig E J, Bandara S and Froese D G 2019 Recent summer warming in northwestern Canada exceeds the Holocene thermal maximum *Nat. Commun.* **10** 1–0
Potter B A, Reuther J D, Holliday V T, Holmes C E, Miller D S and Schmuck N 2017 Early colonization of Beringia and northern North America: chronology, routes, and adaptive strategies *Quat. Int.* **444** 36–55
Putman A L and Bowen G J 2019 A global database of the stable isotopic ratios of meteoric and terrestrial waters *Hydrol. Earth Syst. Sci.* **23** 4389–96
Rohling E J, Foster G L, Grant K M, Marino G, Roberts A P, Tamisiea M E and Williams F 2014 Sea-level and deep-sea-temperature variability over the past 5.3 million years *Nature* **508** 477–82
Rozanski K, Araguásaraguás L and Gonfiantini R 1993 Isotopic patterns in modern global precipitation *Climate Change in Continental Isotopic Records Geophysical Monograph Series* vol 78 ed P K Swart, K C Lohmann, J McKenzie and S Savin (American Geophysical Union) pp 1–36
Schirrmeister L, Meyer H, Andreev A, Wetterich S, Kienast F, Bobrov A, Fuchs M, Sierralta M and Herzschuh U 2016 Late Quaternary paleoenvironmental records from the Chatanika River valley near Fairbanks (Alaska) *Quat. Sci. Rev.* **147** 259–78
Strauss J *et al* 2017 Deep Yedoma permafrost: a synthesis of depositional characteristics and carbon vulnerability *Earth Sci. Rev.* **172** 75–86
Taillandier A S, Domine F, Simpson W R, Sturm M and Douglas T A 2007 Rate of decrease of the specific surface area of dry snow: isothermal and temperature gradient conditions *J. Geophys. Res.* **112** F03003
Throckmorton H M *et al* 2016 Active layer hydrology in an Arctic tundra ecosystem: quantifying water sources and cycling using water stable isotopes *Hydrol. Process.* **30** 4972–86
Vasil'chuk Y K and Budantseva N, A 2021 Holocene ice wedges of the Kolyma Lowland and January paleotemperature reconstructions based on oxygen isotope records *Permafr. periglacial Process.* **33** 3–17
Vasil'Chuk Y K and Vasil'Chuk A C 1997 ^{14}C and ^{18}O in Siberian syngenetic ice-wedge complexes *Radiocarbon* **40** 883–93
Walsh J, E, Chapman W L, Romanovsky V, Christensen J H and Stendel M 2008 Global climate model performance over Alaska and Greenland *J. Clim.* **21** 6156–74
Wetterich S, Meyer H, Fritz M, Mollenhauer G, Rethemeyer J, Kizyakov A, Schirrmeister L and Opel T 2021 Northeast Siberian permafrost ice-wedge stable isotopes depict pronounced Last Glacial Maximum winter cooling *Geophys. Res. Lett.* **48** e2020GL092087
Zazula G D, Froese D G, Elias S A, Kuzmina S and Mathewes R W 2007 Arctic ground squirrels of the mammoth-steppe: paleoecology of Late Pleistocene middens (∼24 000–29 450 ^{14}C yr BP), Yukon Territory, Canada *Quat. Sci. Rev.* **26** 979–1003